PHYSICAL REVIEW E **78**, 055401(R) (2008)

Spatiotemporal moving focus of long femtosecond-laser filaments in air

Ting-Ting Xi,[1,2] Xin Lu,[1] and Jie Zhang[1,3,*]
[1]*Laboratory of Optical Physics, Institute of Physics, Chinese Academy of Sciences, Beijing 100080, China*
[2]*Department of Physics, Graduate University of Chinese Academy of Sciences, Beijing 100049, China*
[3]*Department of Physics, Shanghai Jiao Tong University, Shanghai 200240, China*
(Received 11 June 2007; revised manuscript received 24 April 2008; published 14 November 2008)

The characteristics of filaments formed by femtosecond-laser pulses freely propagating in air are different from those of filaments generated with a focal lens. A scheme combining (2D+1) modeling of the nonlinear Schrödinger equation and ray-tracing method is proposed to provide a fast estimate of the long-range filamentation process in a single-filament regime. A filament with a length of more than 100 m is formed by a 10-mJ, negative chirped 350-fs laser pulse freely propagating in air. A ray-tracing calculation based on the refractive index field obtained from the nonlinear Schrödinger simulation shows that, in the 100-m propagation range, the main mechanism of filamentation is the spatiotemporal moving focus induced by the initial distribution of the laser intensity. The analysis of ray trajectories suggests that the energy exchange between background and filament core due to refocusing of light rays can be induced by Kerr self-focusing without the help of the ionization effect. The plasma defocusing can be observed only at a very short distance on the propagation track, and it prevents the collapse of the laser field.

DOI: 10.1103/PhysRevE.78.055401 PACS number(s): 52.38.Hb, 52.65.−y

The propagation of femtosecond-laser pulses in air opens exciting perspectives for many applications, such as remote sensing, lightning control, and tunable ultrashort-laser-pulse generation [1–3]. Potential applications in turn require a better understanding of the mechanism of filamentation. Many theoretical models have been proposed for the past decade, such as moving focus [4], self-guiding [5], and spatial replenishment models [6]. In the last two models, ionization plays an important role in the formation of filaments. In a long period, most experiments involved in femtosecond-laser filamentation in air used slightly focused pulses to generate filaments in the laboratory scale [7–9]. Such kinds of filaments usually have 100–200 μm diameter and several tens of meters length. The electron generated in this process has a 10^{16}–10^{17} cm^{-3} density, which can clamp the filament intensity down to 10^{14} W/cm^2 [5]. But in view of practical applications, much attention has been focused on the 100-m range filamentation of free propagation of femtosecond-laser pulses in recent years [10–13]. The typical size of filaments in the free propagation is about 1 mm, and the intensity in the filament is just above the ionization threshold. Ionization under this intensity can be estimated using the multiphoton ionization model, only about 10^{13} cm^{-3} [11]. The refractive index change by such a low electron density is several orders lower than that caused by Kerr nonlinearity. In this case the ionization defocusing cannot balance the Kerr self-focusing and here should be other mechanisms underlined in the process of long-range filamentation. In recent years, many femtosecond-laser channeling mechanisms without ionization have been considered [11,14]. In this regard, Méchain *et al.* [11] proposed a propagation regime without ionization based on a very low electron density calculated from the nonlinear Schrödinger (NLS) equation. According to this simulation the saturation mechanism is not ionization, but the broken revolution symmetry in the transverse plane. Later, Kasparian *et al.* [14] performed a ray-tracing calculation for long-range filamentation of femtosecond-laser pulses without taking the ionization effect. This calculation suggests that the long filament results from the moving focus of spatial slices of laser pulses. In that ray-tracing calculation, the laser intensity was obtained from the distribution of rays and the temporal dynamics was not included. However, the effectivity of ray-tracing simulations can be much improved by using a more accurate intensity distribution of the laser field and including other physical processes, such as the ionization effect and temporal dynamics, which can also significantly influence the process of filamentation. Consequently, for a deep understanding of the feature of long-range filamentation of femtosecond-laser pulses, the mechanism still needs to be investigated further.

In this Rapid Communication, we propose a scheme combining a (2D+1) NLS simulation and a spatiotemporal ray-tracing calculation to investigate the mechanism of long-range filamentation by femtosecond-laser pulses freely propagating in air. A filament extending over 100 m is obtained from simulations of the (2D+1) NLS equation. Also, the spatiotemporal distributions of the laser intensity, electron density, and refractive index are calculated. Based on the refractive index field, light rays of different spatiotemporal slices of pulses are traced to model the energy flow in the process of filamentation. For the different spatiotemporal slices, the first focus of light rays occurs at a different distance. This phenomenon suggests that the long filament is formed due to the effect of the spatiotemporal moving focus. After the first focus, the evolution of light rays depends on their incident angles and the intensity distribution of the laser pulse. The evolution causes an energy exchange between the filament and the background.

To describe the free propagation of femtosecond-laser pulses in air, we present simulations on the basis of the (2D+1) NLS equation coupled with the evolution equation

*Author to whom correspondence should be addressed. Fax: +86-10-82649356. jzhang@aphy.iphy.ac.cn

of electron density. The NLS equation governs a slow envelop of the laser electric field E in the frame moving with group velocity v_g $(t \rightarrow t - z/v_g)$. The coupled equations can be written as

$$\frac{\partial E}{\partial z} = i\frac{1}{2k_0}\Delta_\perp E - i\frac{k''}{2}\frac{\partial^2 E}{\partial t^2} + ik_0 n_2 |E|^2 E - ik_0 \frac{n_e}{2n_c} E - \frac{\beta^{(K)}}{2}|E|^{2K-2}E, \quad (1)$$

$$\frac{\partial n_e}{\partial t} = \frac{\beta^{(K)}}{K\hbar\omega_0}|E|^{2K}\left(1 - \frac{n_e}{n_{at}}\right). \quad (2)$$

Here $k_0 = 2\pi/\lambda_0$ ($\lambda_0 = 800$) nm is the central wave number. The coordinate of Eq. (1) is cylindrically symmetric, and the Laplacian operator $\Delta_\perp = \frac{\partial^2}{\partial r^2} + \frac{1}{r}\frac{\partial}{\partial r}$ denotes the beam transverse diffraction. Group-velocity dispersion is also included with coefficient $k'' = 0.2$ fs^2/cm. The remaining terms represent the Kerr self-focusing with coefficient $n_2 = 3.2 \times 10^{-19}$ cm^2/W, electron defocusing, and multiphoton absorption with coefficient of $\beta^{(K)} = 3.1 \times 10^{-98}$ cm^{13}/W^7 for the number of photons $K = 8$. The electron in Eq. (2) is generated by multiphoton ionization of air. The critical plasma density and the neutral atom density are $n_c = 1.7 \times 10^{21}$ cm^{-3} and $n_{at} = 5.4 \times 10^{18}$ cm^{-3}, respectively.

Equation (1) is solved by use of the fast Fourier transform in time and Crank-Nicholson scheme in space. A Gaussian profile is used to model the initial laser pulse $E(r,t,z=0) = (2P_{in}/\pi w_0^2)^{1/2}\exp(-r^2/w_0^2 - t^2/\tau_0^2 - ict^2/\tau_0^2)$, where the laser pulse has an energy of 10 mJ, a peak power $P_{in} = 27$ GW, a transverse waist [full width at half maximum (FWHM)] $w = \sqrt{2\ln 2}w_0 = 10$ mm, and a temporal duration (FWHM) $\tau = \sqrt{2\ln 2}\tau_0 = 350$ fs with negative chirp $c = -5.75$. In the simulation, we divide the temporal region with the grid number 1024 and the resolution is 1.74 fs. In the radial direction, we adopt a nonuniform grid division. The spatial resolution is 18.4 μm in the filament region and 111 μm in the fringe. Correspondingly, the number of spatial grids N_r is 600. The Crank-Nicholson scheme we used is stable without any additional conditions. The grid size of the propagation direction is 1.5 mm, which is defined to guarantee convergence of the algorithm. Figure 1 shows the distributions of the energy fluence (a), peak intensity (b), and peak electron density (c) for the laser pulse propagating in air. A stable filament is formed and extends more than 100 m. During this process, the peak intensity of the filament reaches 8.1×10^{13} W/cm^2. The effective ionization is only observed at a few short distances, and the maximum of the electron density is 4.9×10^{16} cm^{-3}.

Simulations of the coupled NLS equations provide the distribution of the energy fluence and intensity of the laser pulse. To obtain an intuitive picture of this distribution, we carry out ray-tracing studies based on the refractive index field from numerical solution of the NLS equation. The propagation of the laser pulse is considered as a bunch of light rays. The trajectory of each ray can be described by

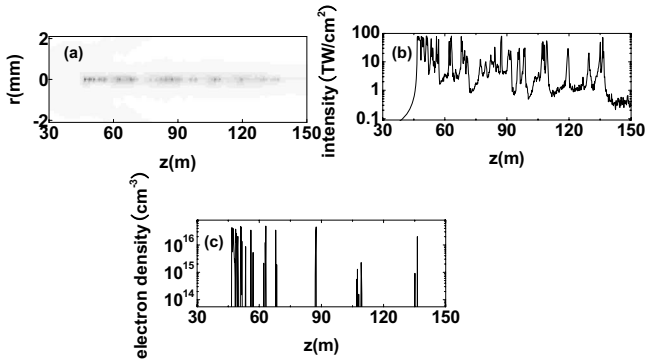

FIG. 1. (a) Energy fluence distribution, (b) peak intensity, and (c) peak electron density of the femtosecond-laser filament as a function of propagation distance z.

$$\frac{d^2 r}{dz^2} = \nabla\eta, \quad (3)$$

where r is the position of the light rays and z is the propagation distance. The refractive index of air η is given by

$$\eta = n_0 + n_2 I - \frac{n_e}{2n_c}, \quad (4)$$

where the n_0 is linear part, whose value is constant, and the nonlinear parts $n_2 I$ and $n_e/2n_c$ are induced by the Kerr effect and ionization, respectively. To obtain the precise evolution of light rays, the values of the intensity $I(r,t,z)$ and electron density $n_e(r,t,z)$ in Eq. (4) are obtained from the simulation results of the NLS equation.

Since $\nabla n_0 = 0$, the evolution of light rays depends on the distribution of the refractive index contributed by Kerr nonlinearity and ionization. Here we compare the contribution of the Kerr nonlinearity and electron density to the refractive index for different time slices of the laser pulse. Figure 2 shows the distribution of the nonlinear refractive index induced by Kerr nonlinearity ($n_2 I$) and electrons ($n_e/2n_c$) for time slices $t = -174$ fs (a), 0 fs (b), and 174 fs (c). A comparison between the maxima of $n_2 I$ and $n_e/2n_c$ in Fig. 2 is

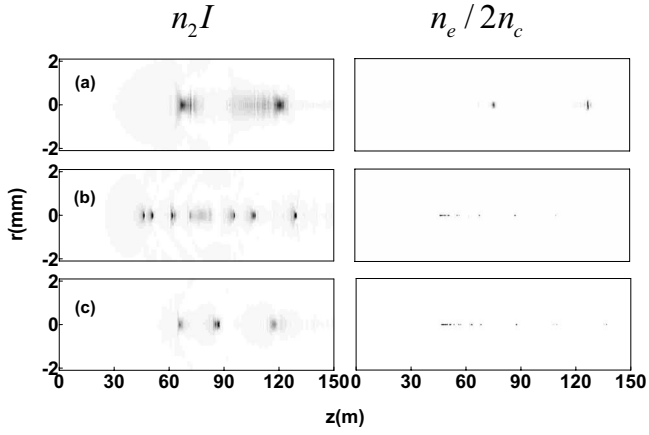

FIG. 2. The nonlinear refractive index induced by the Kerr effect (left) and electrons (right) for time slices $t = -174$ fs (a), 0 fs (b), and 174 fs (c).

TABLE I. The maxima of the refractive index contributed by the Kerr effect and ionization for time slices $t=-174$ fs, 0 fs, and 174 fs.

t	$(n_2I)_{max}$	$(n_e/2n_c)_{max}$
−174 fs	4.5×10^{-7}	1.1×10^{-17}
0 fs	1.4×10^{-5}	1.4×10^{-5}
174 fs	2.1×10^{-6}	1.4×10^{-5}

shown in Table I. We can see that n_2I is much larger than $n_e/2n_c$ for time slices at the leading edge. At the trailing edge, the maximum of $n_e/2n_c$ is larger than that of n_2I. However, the electrons are generated only at a few short distances. For most of the laser pulses, n_2I is much larger than $n_e/2n_c$. The results suggest that the effect of ionization on the formation of long filaments should be much weaker than the Kerr nonlinearity.

From each transverse numerical grid in simulations of the NLS equation, we launch one ray, the initial direction of which is parallel to the beam axis. Figure 3 shows the trajectory of light rays for the time slices $t=-174$ fs (a), 0 fs (b), and 174 fs (c) in the refractive index fields $\eta=n_0+n_2I-\frac{n_e}{2n_c}$ (left) and $\eta=n_0+n_2I$ (right). First, we investigate the trajectory of light rays when both the effects of Kerr nonlinearity and ionization are considered ($\eta=n_0+n_2I-n_e/2n_c$), as shown in Fig. 3 (left). For different time slices, the common feature of light rays is that the rays from different start positions arrived at the beam axis at different propagation distances. And the focusing distance of rays essentially increases with their initial distance from the beam axis, similar to the results in Ref. [14]. Central rays with higher intensity focus earlier than rays in the fringe. Thus, it can be concluded that the effect of a moving focus can also be induced by the spatial distribution of the laser intensity. During this process, the background energy replenishes the filament core

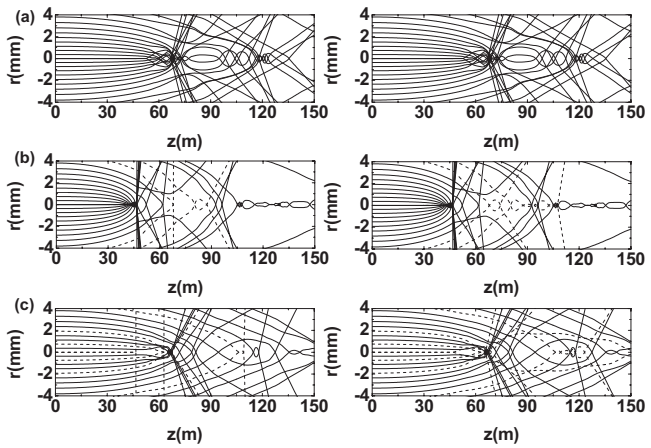

FIG. 3. The evolution of light rays for time slices $t=-174$ fs (a), 0 fs (b), and 174 fs (c) when both the effects of Kerr nonlinearity and electrons are considered (left) and only the Kerr nonlinearity is included (right).

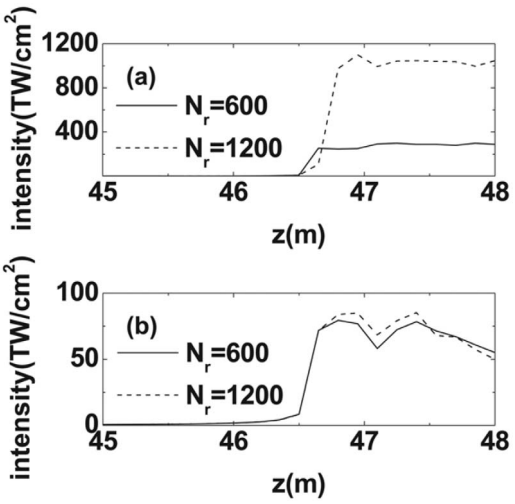

FIG. 4. The peak intensity of the femtosecond-laser pulse without (a) and with (b) taking account of ionization in simulations of the NLS equation. Simulations are performed for two different spatial grid numbers $N_r=600$ (solid line) and 1200 (dashed line).

over the propagation distance. The mechanism of this kind of moving focus is described in Ref. [14]. From Fig. 3 (left) we can see that after the crossing with the beam axis, some rays escape the beam, but some rays can be trapped by the gradient of the refractive index and return to the filament core again. The trajectory of rays is dependent on the incident angle of the beam axis and refractive index distribution. Comparing the trajectories of light rays with and without taking account of the ionization effect ($n_e/2n_c$), as shown in Fig. 3 (left) and Fig. 3 (right), we can see they are almost the same except for a few rays, which are drawn as dashed lines in Fig. 3. At some propagation distance the ionization effect is able to change the direction of rays when the rays approach the beam axis. However, electrons are generated at a few short distances and only influence the laser field very close to the filament core.

To investigate further the role of ionization in the free propagation, we compare the peak intensities of the femtosecond-laser pulse with and without taking account of ionization in simulations of the NLS equation, as shown in Fig. 4. Two different spatial grid numbers ($N_r=600$ and 1200) are used in the simulations. Figure 4(a) shows that when ionization is not considered, the intensity of the laser pulse at the first focus ($z=46.5$ m) increases quickly with enhancement of the spatial resolution. However, the spatial resolution does not significantly influence the peak intensity when the ionization is considered, as shown in Fig. 4(b). The results suggest that without ionization, the laser beam will collapse. However, in the free propagation, the electrons are generated only at a few short distances. The region where plasma defocusing plays an important role is small. Actually, when the femtosecond-laser pulse propagates in natural air, the air turbulence widens the diameter of the filament to mm size; in this case, the electron density becomes many orders lower and the role of ionization can be quite negligible [15].

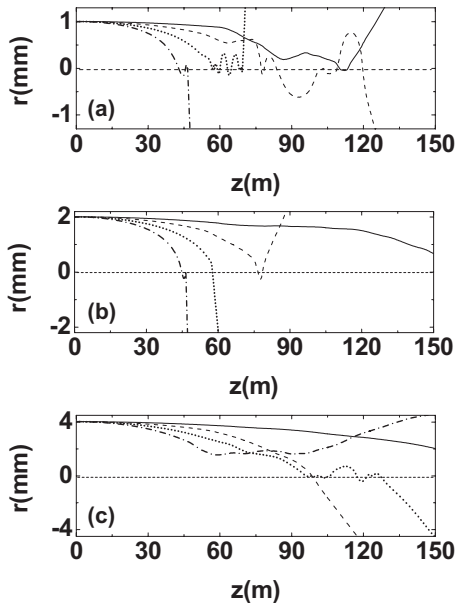

FIG. 5. The evolution of light rays with initial positions r_0 =1 mm (a), 2 mm (b), and 4 mm (c) for time slices t=−278 fs (solid line), −209 fs (dashed line), −139 fs (dotted line), and 0 fs (dash-dotted line).

In the macroscopic scale, ionization does not play a critical role in the formation of long filaments.

In order to analyze the temporal effect of laser pulses on long-filament formation, we carry out a ray-tracing simulation for 20 time slices from the front edge to the trailing edge of the laser pulse. Figure 5 shows the trajectory of light rays with initial positions r_0=1 mm (a), 2 mm (b), and 4 mm (c) for different time slices. For clarity, the figure only displays light rays from four time slices. It can be seen that for the same starting position, the rays of different time slices also approach the beam axis at different distances. The rays from more intense time slices focus on the earlier propagation distance. These results are in good agreement with the model of moving focus proposed by Brodeur *et al.* [4]. Thus, we can see that the spatiotemporal moving focus induced by the initial profile of the laser pulse is the dominating process for the formation of long filaments.

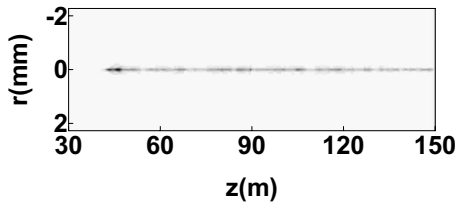

FIG. 6. The energy fluence distribution transferred from the ray-tracing results.

To test the reliability of the ray-tracing method, we transfer the evolution of light rays to the fluence distribution (Fig. 6). The fluence is integrated from the 20 time slices we have calculated. Comparing Figs. 6 and 1, we can see that the ray-tracing results are in good agreement with the numerical solution of the NLS equation in terms of filament length, size, and onset position. But there are still some slight differences between the ray-tracing calculation and modeling the NLS equation. The main reason is that the group velocity and diffraction effect of rays are not considered and the resolution of time slices is not high enough.

In conclusion, the mechanism of long-range filamentation of femtosecond-laser pulses in air is investigated by a combination of NLS simulations and ray-tracing calculations. The contribution of the Kerr effect and ionization to the refractive index of air was quantitatively analyzed and compared. The ray-tracing simulations show that a long filament is basically formed due to the moving focus induced by the initial distribution of the laser intensity in the spatial and temporal domains. The Kerr self-focusing is the dominant process during filamentation of the freely propagating laser pulse. But the ionization effect is still needed for suppression of laser collapse at nonlinear focuses, which is distributed only at a few short distances. The self-guided mechanism due to the dynamic balance between Kerr self-focusing and ionization defocusing may take place for filamentation of prefocused laser pulses in air or filamentation in solid and liquid media, where the electron density is much higher.

This work was supported by the National Natural Science Foundation of China under Grants No. 10734130, No. 10634020, and No. 60621063, National Basic Research Program of China (973 Program) (Grant No. 2007CB815101), and the National Hi-tech ICF Program.

[1] J. Kasparian *et al.*, Science **301**, 61 (2003).
[2] R. Ackermann *et al.*, Appl. Phys. Lett. **85**, 5781 (2004).
[3] F. Théberge *et al.*, Phys. Rev. Lett. **97**, 023904 (2006).
[4] A. Brodeur *et al.*, Opt. Lett. **22**, 304 (1997).
[5] A. Braun *et al.*, Opt. Lett. **20**, 73 (1995).
[6] M. Mlejnek *et al.*, Opt. Lett. **23**, 382 (1998).
[7] S. Tzortzakis *et al.*, Phys. Rev. Lett. **86**, 5470 (2001).
[8] G. Méchain *et al.*, Phys. Rev. Lett. **93**, 035003 (2004).
[9] Z. Q. Hao *et al.*, Opt. Express **14**, 773 (2006).
[10] M. Rodriguez *et al.*, Phys. Rev. E **69**, 036607 (2004).
[11] G. Méchain, *et al.*, Appl. Phys. B: Lasers Opt. **79**, 379 (2004).
[12] F. Théberge *et al.*, Appl. Phys. Lett. **87**, 081108 (2005).
[13] G. Méchain *et al.*, Opt. Commun. **247**, 171 (2005).
[14] J. Kasparian *et al.*, Appl. Phys. B: Lasers Opt. **79**, 947 (2004).
[15] Y. Y. Ma *et al.*, Opt. Express **16**, 8332 (2008).